Models for dynamic correlated charge collection effects in thick CCDs

Conference or Workshop Item

Models for dynamic correlated charge collection effects in thick CCDs

Daniel P. Weatherill[a], Konstantin D. Stefanov[a], Andrew D. Holland[a], Douglas Jordan[b], Ivan V. Kotov[c]

[a]Centre for Electronic Imaging, The Open University, Milton Keynes, MK7 6AA, UK;
[b]e2v Technologies Limited, 106 Waterhouse Lane, Chelmsford, CM1 2QU, UK ;
[c]Brookhaven National Laboratory, Brookhaven Avenue, Upton, NY 11973, USA

ABSTRACT

Dynamic charge collection effects in thick CCDs have received interest in recent years, due to the performance implications for both ground and space based precision optical astronomy. The phenomena manifest as the "brighter - fatter" effect in Point Spread Function (PSF) measurements, and nonlinearity and signal dependence in spatial autocorrelation and photon transfer measurements. In this paper we present validation results from simple, analytically based predictive models for this effect, using an e2v CCD250. The model is intended to provide estimations for predicting device performance based on design parameters.

Keywords: CCD, Deep Depletion, Brighter Fatter Effect, Charge Collection, Modelling, Poisson Equation

1. INTRODUCTION

Dynamic effects on charge collection in sensors in general, and the "brighter-fatter effect" (hereafter: BFE) in particular are becoming ever more important; being strongly exhibited in thick, fully depleted, back biased CCDs such as the e2v CCD250 LSST sensor candidate device, and having been observed also in testing of CCD273 devices for the ESA Euclid mission[1–4] .

Much work has been carried out in recent years to address both the cause and correction of the BFE. The phenomenon is correctly understood as being caused by changes in the drift field structure of CCD pixels in response to stored charge. This results in the apparent shifting of pixel geometrical boundaries as signal is accumulated. A detailed modelling and measurement framework based on dynamic pixel boundaries has recently been developed,[5] which shows how accurate coefficients for a first-order electrostatic model of the boundary shifts can be extracted from calibration data. Electrostatic drift calculations have also been used to give good agreement in explaining both the BFE and other static effects related to stored or trapped charge in the device volume.[6]

In this contribution we introduce a physically-motivated model of the parallel transfer direction in a thick, back biased CCD based on analytical solutions of Poisson's equation, which can be used to efficiently predict pixel boundary shifts based on device design parameters and operating conditions. A similar approach may be useful in treating the serial direction, though it is not addressed in this work. The model is potentially useful in device design, or when assessing possible performance of different sensors in telescope design studies.

2. CALCULATING CHARGE STORAGE DEPTH

A full analytical description of the buried channel CCD in 2D (or 3D) including the effects of stored charge would necessitate simultaneous solution of Poisson's equation and the electron drift-diffusion and continuity equations, and would certainly be intractable. Previous electrostatic models used to explain the BFE have assumed a point charge[4] for the storage, and we wish to relax this assumption slightly without greatly over-complicating the model. The approximation used is to first assume that the charge distribution is abrupt and that doping levels are constant, and that the depletion layer approximation applies, so the background charge in the silicon can be represented as "blocks" of charge (see Figure 2). Under these conditions, the potential in a 1D MOS device,

Corresponding Author: Daniel P. Weatherill, E-mail: daniel.weatherill@open.ac.uk, telephone: +44 (0) 1908 653444

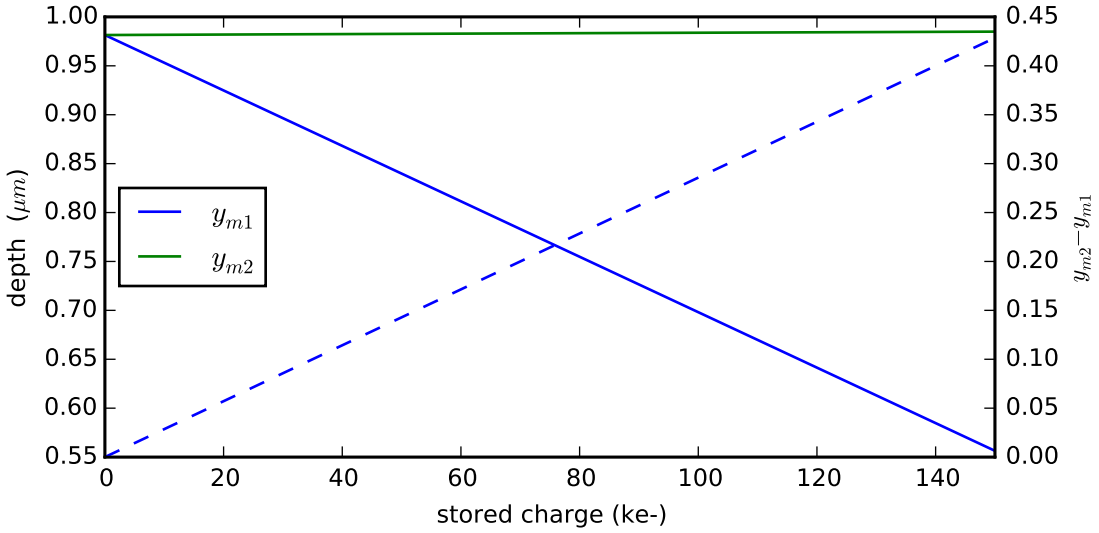

Figure 1. Storage depths of charge packets from the 1D model. The difference between y_{m1} and y_{m2} is shown by the dashed line

including stored charge, can be exactly solved, using the formulae derived by Yin and Cooper,[7] which can easily be adjusted to include a fixed depletion depth, as shown in.[8] It would be possible to use a more realistic charge distribution, at the cost of not being able to solve the model analytically. In principle, an arbitrary charge distribution may be used in the 2D model described in section 3 below. The 1D model is used to calculate the storage depth parameters y_{m1} and y_{m2} given the storage density Q. The further assumption we make is that the density of the charge packet, ρ, will be buried

$$\rho = \frac{-q \cdot N_D}{(y_{m2} - y_{m1}) \cdot L \cdot B} \tag{1}$$

where q is the charge on an electron, N_D is the number density of donors , L is the collecting gate width (also assuming no gaps between collecting gates), and B is the distance between channel stops. The obvious implication of this assumption is that blooming of charge is not an effect included in the model. The storage density can then be calculated by

$$Q = \frac{Q_0}{L \cdot B} \tag{2}$$

where Q_0 is the charge (in units of electrons) we wish to store in the pixel. The relationship between y_{m1}, y_{m2} and Q is shown in Figure 1.

Other parameters required to construct the model are N_A, the number density of acceptors,y_T the device thickness and y_j the junction depth. N_A may be estimated from the reported resistivity of the device,[9] and y_j may be estimated by measuring the channel potential of the device, and then adjusting the y_j parameter of Yin and Cooper's model to obtain agreement. This technique is nevertheless rather inaccurate, but of course may be much better estimated in the context of a device designer, knowing the doping parameters used in construction. In the following work, we use the values $N_D = 1 \times 10^{16}\,\mathrm{cm}^{-3}$, $N_A = 5 \times 10^{12}\,\mathrm{cm}^{-3}$ and $y_j = 1.0\,\mu\mathrm{m}$. A schematic diagram of the device is shown in Figure 3

3. ANALYTIC MODELLING OF CCD PIXELS

Some of the basis for the approach of our model has been previously published,[8] but several notable refinements to the previous approach which will be highlighted and discussed. In particular, it was found that the original approach to incorporating charge storage into a 2D model of a CCD pixel was insufficiently realistic to closely

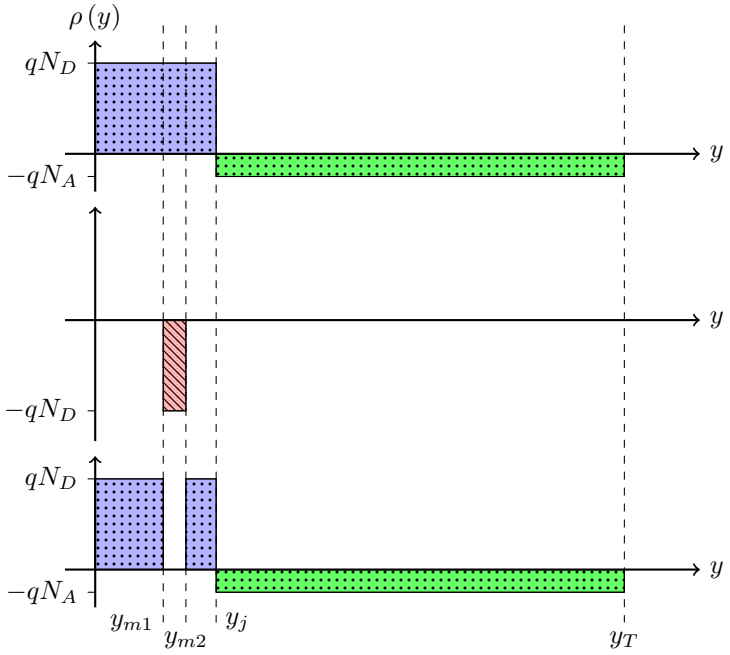

Figure 2. The assumed 1D charge distribution within a pixel top: the dopants, middle: stored electrons, bottom: resulting charge distribution

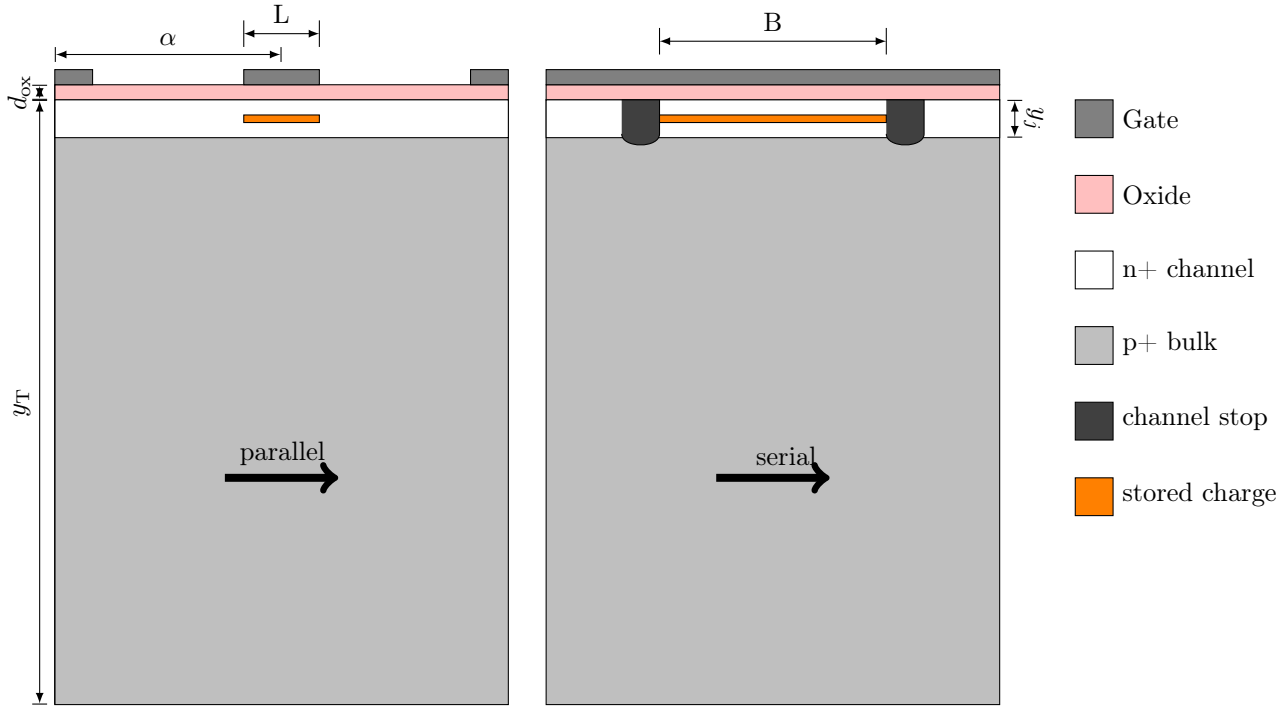

Figure 3. Schematic diagram of a CCD. Only the gates which are high during collection (at V_G) are shown.

reproduce the observed effects in experimental data. We shall therefore recap the development of the 2D analytical model here.

In order to investigate the collection of electrons in a CCD, a solution to the Poisson equation

$$\nabla^2 \Phi = \frac{N(y) + n(x,y)}{\epsilon(y)\,\epsilon_0} \tag{3}$$

where Φ is the potential, $N(y)$ is the fixed charge distribution due to ionised dopants, $n(x,y)$ is the stored electron charge distribution, $\epsilon(y)$ is the relative permittivity, and ϵ_0 is the permittivity of free space. The solution for Φ is subject to the boundary conditions imposed by the gate potentials:

$$\Phi(x,y) = \begin{cases} V_G & -\frac{L}{2} < x < \frac{L}{2} \\ V_T & \text{elsewhere} \end{cases} \tag{4}$$

with V_G the high gate voltage, and V_T the low gate voltage (i.e. the "front substrate" voltage). Both of these are referenced relative to the substrate at the back surface, taken to be $V_{SS} = 0$. Thus, a device with a back-side bias of $-70\,\mathrm{V}$, and collecting gate voltage of $15\,\mathrm{V}$ corresponds to the values $V_G = 85\,\mathrm{V}$, $V_T = 70\,\mathrm{V}$. The potential is considered to be written as the sum of three distinct components:

$$\Phi = \Phi_H + \Phi_P + \Phi_C \tag{5}$$

where Φ_H is the homogeneous solution (i.e. a solution which satisfies the boundary conditions in (4) but does not include the charge distribution) which is as derived by Lester and Pulfrey.:[10]

$$\Phi_H = V_T + \frac{V_G - V_T}{\pi}\left(\tan^{-1}\left(\frac{y + d_{\mathrm{ox}}}{x - \frac{L}{2}}\right) - \tan^{-1}\left(\frac{y + d_{\mathrm{ox}}}{x + \frac{L}{2}}\right)\right) \tag{6}$$

where d_{ox} is the oxide layer thickness, and L is the collecting gate width. Φ_P is a particular integral solution, which satisfies vanishing boundary conditions and accounts for the dopant charge density. For a fully depleted device, where the potential is also forced to obey the boundary condition

$$\Phi(x,T) = 0 \tag{7}$$

by virtue of the biasing conditions, the calculation of Φ_P is somewhat simpler than the iterative procedure described by Lester and Pulfrey[10] for a device without full depletion, since the depletion depth is constant, and is equal to the thickness of the device, y_T. For this situation (and for values of $y \geq y_j$) , the particular integral may be written as

$$\Phi_P(x,y) = \frac{-q y_j}{\epsilon_s \epsilon_0}\left(\frac{N_D}{2} + N_A\right)\cdot y + \frac{q \cdot y_j^2}{2 \cdot \epsilon_s \cdot \epsilon_0}\left(N_D + N_A\right)^2 + C(x)\cdot\left(\frac{\epsilon_o}{\epsilon_s}\cdot y + d_{\mathrm{ox}}\right) \tag{8}$$

$$\text{where}\quad C(x) = \frac{q}{\epsilon_o \cdot y + \epsilon_s \cdot d_{\mathrm{ox}}}\left(-y_j \cdot y_T\left(\frac{N_D}{2} + N_A\right) + \frac{y_j^2}{2}\left(N_D + N_A\right) + \frac{\epsilon_s}{\epsilon_0}\cdot \Phi_H(x,T)\right) \tag{9}$$

Finally, Φ_C is a potential added to incorporate the stored charge. We find this using the Green's function. The fundamental solution $G_0(x,y;x',y')$ for the 2D Poisson equation is well known,[11] and given by:

$$G_0(x,y;x',y') = \frac{1}{4\cdot\pi}\ln\left(\left(x - x'\right)^2 + \left(y - y'\right)^2\right) \tag{10}$$

so that the solution for Φ_C on an unbounded domain is:

$$\Phi_C^{\infty}(x,y) = \frac{-q \cdot N_D}{4 \cdot \pi \cdot \epsilon_s \epsilon_0}\int_{-\frac{L}{2}}^{\frac{L}{2}}\int_{y_{m1}}^{y_{m2}} \ln\left(\left(x - x'\right)^2 + \left(y - y'\right)^2\right)\cdot dy' \cdot dx' \tag{11}$$

where y_{m1} is the shallow limit of charge storage and y_{m2} is the deep limit (which were found for a certain stored charge Q_0 using the 1D model described in Section 2).

We may then use the method of images to construct a solution for Φ_C on the bounded domain presented by the pixel (i.e. the two parallel plates at $y = 0$ and $y = y_T$), which results in

$$\Phi_C(x,y) = \frac{-q \cdot N_D}{4 \cdot \pi \cdot \epsilon_s \epsilon_0} \sum_{n=-\infty}^{\infty} \left(\int_{-\frac{L}{2}}^{\frac{L}{2}} \int_{y_{m1}}^{y_{m2}} \ln\left((x-x')^2 + (2 \cdot n \cdot y_T + y - y')^2 \right) \cdot dy' \cdot dx' \right) + \frac{q \cdot N_D}{4 \cdot \pi \cdot \epsilon_s \epsilon_0} \sum_{n=-\infty}^{\infty} \left(\int_{-\frac{L}{2}}^{\frac{L}{2}} \int_{y_{m1}}^{y_{m2}} \ln\left((x-x')^2 + (2 \cdot n \cdot y_T - y - y')^2 \right) \cdot dy' \cdot dx' \right) \quad (12)$$

At first glance, this expression appears rather unwieldy. Indeed, the series converges quite slowly, and calculating the infinite sum of double integrals (or, equivalently, the double integral of the infinite sum) to appropriate precision is computationally expensive. However, in all of the modelling calculations which follow (except for production of figures showing the shape of potentials), the relevant quantity is not the potential but the field components, $E_{C,x} = -\frac{\partial \Phi_C}{\partial x}$ and $E_{C,y} = -\frac{\partial \Phi_C}{\partial y}$. Note that due to the symmetry of the Green's function, differentiating under the integral effectively means that calculating the field components requires only a single integration,

$$E_{C,x} = \frac{-q \cdot N_D}{4 \cdot \pi \cdot \epsilon_s \epsilon_0} \cdot \sum_{n=-\infty}^{\infty} \int_{y_{m1}}^{y_{m2}} \left[\ln\left((x-x')^2 + (2 \cdot n \cdot y_T + y - y')^2 \right) \right]_{-\frac{L}{2}}^{\frac{L}{2}} \cdot dy' + \frac{q \cdot N_D}{4 \cdot \pi \cdot \epsilon_s \epsilon_0} \cdot \sum_{n=-\infty}^{\infty} \int_{y_{m1}}^{y_{m2}} \left[\ln\left((x-x')^2 + (2 \cdot n \cdot y_T - y - y')^2 \right) \right]_{-\frac{L}{2}}^{\frac{L}{2}} \cdot dy' \quad (13)$$

$$E_{C,y} = \frac{-q \cdot N_D}{4 \cdot \pi \cdot \epsilon_s \epsilon_0} \cdot \sum_{n=-\infty}^{\infty} \int_{-\frac{L}{2}}^{\frac{L}{2}} \left[\ln\left((x-x')^2 + (2 \cdot n \cdot y_T + y - y')^2 \right) \right]_{y_{m1}}^{y_{m2}} \cdot dx' + \frac{q \cdot N_D}{4 \cdot \pi \cdot \epsilon_s \epsilon_0} \cdot \sum_{n=-\infty}^{\infty} \int_{-\frac{L}{2}}^{\frac{L}{2}} \left[\ln\left((x-x')^2 + (2 \cdot n \cdot y_T - y - y')^2 \right) \right]_{y_{m1}}^{y_{m2}} \cdot dx' \quad (14)$$

By using the definition of logarithms of complex numbers, these integrals can be evaluated directly, giving

$$E_{C,x} = \frac{-q \cdot N_D}{4 \cdot \pi \cdot \epsilon_s \epsilon_0} \cdot \sum_{n=-\infty}^{\infty} \left(\Upsilon\left(x, 2 \cdot n \cdot y_T + y, -\frac{L}{2}, \frac{L}{2}, y_{m1}, y_{,m2} \right) - \Upsilon\left(x, 2 \cdot n \cdot y_T - y, -\frac{L}{2}, \frac{L}{2}, y_{m1}, y_{m2} \right) \right) \quad (15)$$

$$E_{C,y} = \frac{-q \cdot N_D}{4 \cdot \pi \cdot \epsilon_s \epsilon_0} \cdot \sum_{n=-\infty}^{\infty} \left(\Upsilon\left(2 \cdot n \cdot y_T + y, x, y_{m1}, y_{,m2}, -\frac{L}{2}, \frac{L}{2} \right) - \Upsilon\left(2 \cdot n \cdot y_T - y, x, y_{m1}, y_{,m2}, -\frac{L}{2}, \frac{L}{2} \right) \right) \quad (16)$$

where the function $\Upsilon(\alpha, \beta, \alpha_l, \alpha_h, \beta_l, \beta_h)$ is given by:

$$\Upsilon(\alpha, \beta, \alpha_l, \alpha_h, \beta_l, \beta_h) = 2 \cdot \left(\beta_h \cdot \ln\left| \frac{z_{hh}}{z_{lh}} \right| + \beta_l \cdot \ln\left| \frac{z_{ll}}{z_{hl}} \right| \right) + z_h^* \cdot \ln\left(\frac{z_{hl}}{z_{hh}} \right) + z_h \cdot \left(\ln\left(\frac{z_{hl}}{z_{hh}} \right) \right)^* + z_l^* \cdot \ln\left(\frac{z_{lh}}{z_{ll}} \right) + z_l \cdot \left(\ln\left(\frac{z_{lh}}{z_{ll}} \right) \right)^* \quad (17)$$

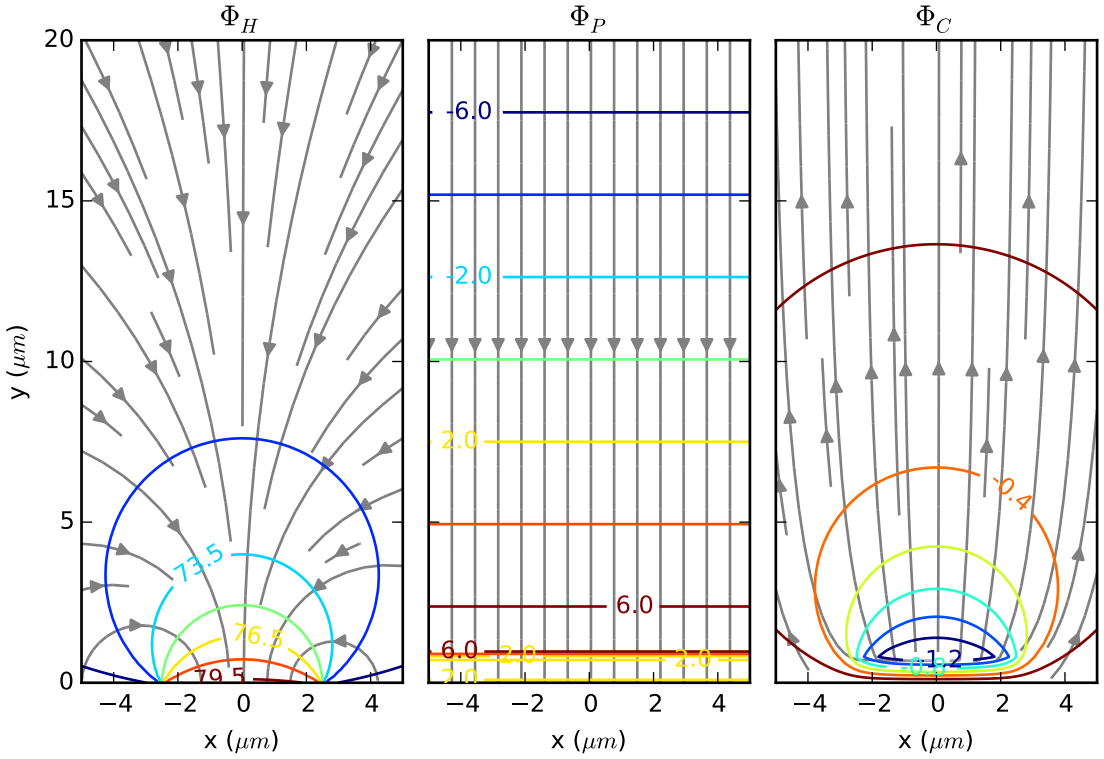

Figure 4. Potential solution components: Contour lines show the potential arising from the homogeneous (Φ_H), particular (Φ_P) and stored-charge (Φ_C) components. The streamlines show electron drift trajectories under constant mobility (i.e. they follow the opposite vector direction to the electric field) arising from each component. Note that the contour line steps differ between plots.

with:

$$z_h = \beta + \hat{\imath}\,|\alpha - \alpha_h|\,; \quad z_l = \beta + \hat{\imath}\,|\alpha - \alpha_l|$$
$$z_{hh} = -\beta + \beta_h + \hat{\imath}\,|\alpha - \alpha_h|\,; \quad z_{lh} = -\beta + \beta_h + \hat{\imath}\,|\alpha - \alpha_l|$$
$$z_{hl} = -\beta + \beta_l + \hat{\imath}\,|\alpha - \alpha_h|\,; \quad z_{ll} = -\beta + \beta_l + \hat{\imath}\,|\alpha - \alpha_l|$$

where $\hat{\imath}$ is the imaginary unit, and the symbol z^* represents the complex conjugate of z. It is simple to verify using elementary properties of complex numbers that the range of the function Υ includes only the real numbers. We find that the evaluation of the single integral of the infinite series can be performed efficiently to acceptable accuracy using the Levin u-transform technique,[12] as implemented in the GNU Scientific Library.[13]

The various components of the potential and field solutions for a single pixel and how they combine are illustrated in Figure 4.

The extension of the single pixel solution to multiple pixels is achieved by computing the Fourier series of the Homogeneous and Particular parts of the potential. The homogeneous multipixel potential Φ'_H is given by:

$$\Phi'_H(x,y) = \frac{a_0}{2} + \sum_{n=1}^{\infty} a_n(x,y) \cdot \cos\left(\frac{2n\pi x}{\alpha}\right) \cdot dx \tag{18}$$

$$\text{with} \quad a_n(x,y) = \frac{2}{\alpha}\int_{-\frac{\alpha}{2}}^{\frac{\alpha}{2}} \Phi_H(x,y) \cdot \cos\left(\frac{2n\pi x}{\alpha}\right) \cdot dx \tag{19}$$

where the inter-pixel spacing is given by α, and only the cosine terms are required because Φ_H is an even function (cf. (6)). The particular potential Φ_P is only very weakly dependant on x, and even then the x

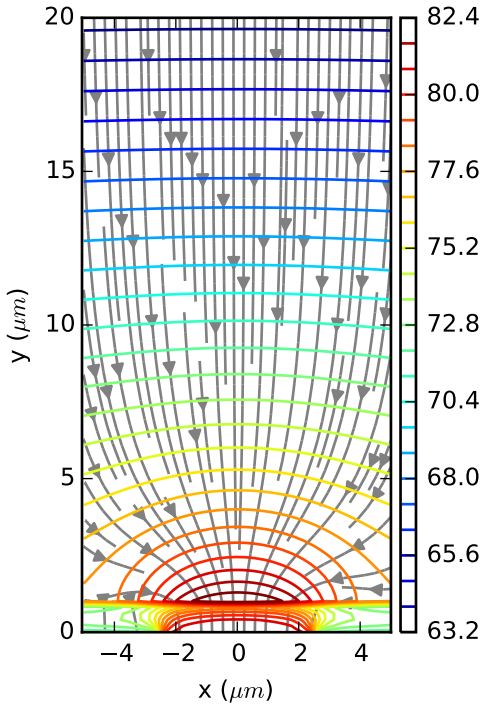

Figure 5. Combined single pixel summed solution, showing the potential (contour lines) and resultant electron drift trajectories (streamlines).

dependency is only introduced by $\Phi_H(x, y_T)$ (see (9)). So, although the Fourier series is rather unwieldy to evaluate (especially given the y position dependence of a_n), a single calculation serves for both the homogeneous and particular potentials. Again, we find the Levin u-transform invaluable in calculating this series, though particular care must be taken to preserve numerical hygeine when choosing which terms to include in the truncated series, due to the evaluation of the arctangent function at very high (though not infinite) values, implied by the components near $x = \pm\frac{L}{2}$. The channel charge potential Φ_C is then added to the solution. In principle, this allows the evaluation of boundary shifts given arbitrary stored charge distributions over many pixels. An interesting principle case to examine is that with a charge in the central pixel and none in the others (see Figure 6)

4. PIXEL BOUNDARY CALCULATIONS

The boundary of a pixel is found numerically using the Brent minimization method, again as implemented in GSL, to locate the zero crossing of the x-going electric field. Some examples of calculated boundary shifts are shown in Figure 7. These boundary shifts are for the boundary nearest the stored charge, and as expected, the shift is inwards, so that the pixel containing the charge becomes smaller. This quantity is referred to by Guyonnet et al[5] as $\delta^0_{0,0}$. The shape of the boundaries supports the evidence observed by most authors that the BFE is almost achromatic, (i.e. the boundary does not move much beyond the first few μm of the device). However, the curvature of the boundary does appear to increase with higher stored charge, so it is possible that chromaticity becomes a more relevant factor for devices near saturation.

We can also readily calculate an average over depth for the boundary (neglecting the first few microns of device), and find that the value of $\delta^0_{0,0}$ against stored charge is well fit by a quadratic equation (see Figure 8). In observations of BFE, it is generally reported that the correlations measured increase linearly with signal,[14] and from the model of Antilogus et al,[4] we see that this is used to justify a linear model between boundary shifts $\delta_{i,j}$

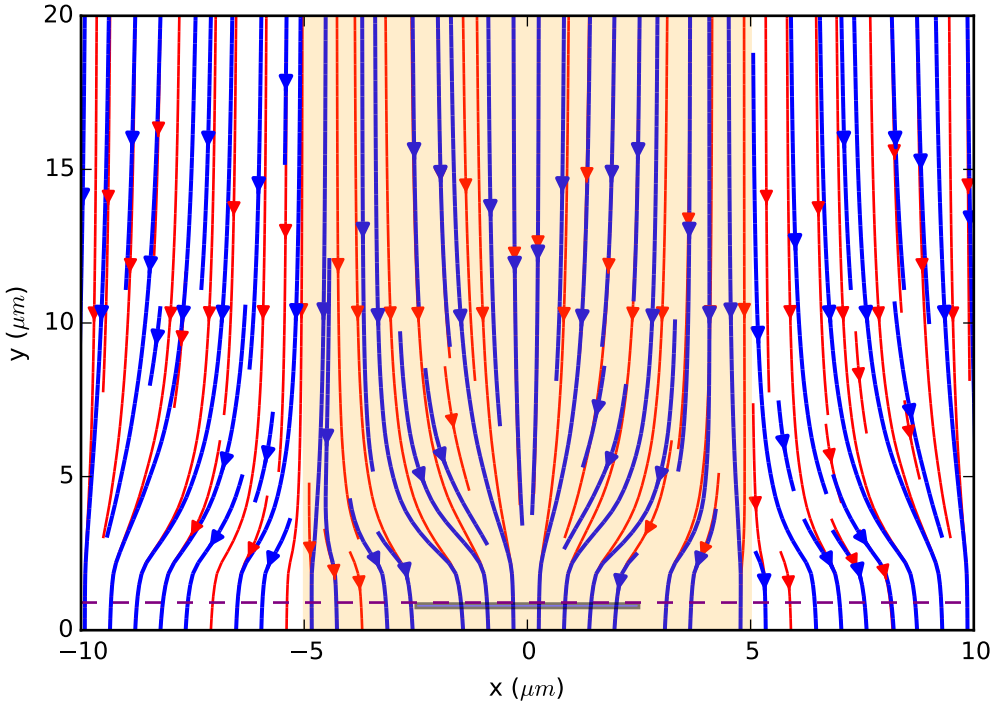

Figure 6. Driftlines of a multipixel solution. The thinner (red) lines show the central pixel containing 10ke$^-$ of charge, and the thicker (blue) lines show 50ke$^-$. The dashed purple line indicates the junction depth, the shaded central region the geometrical pixel boundary, and the coloured box the location of the stored charge.

and constant coefficients a_{ij}:

$$\frac{\delta^X_{i,j}}{p} = \frac{Q_{i,j}a^X_{i,j}}{2} \tag{20}$$

it should be noted here that in the fits we have calculated, the quadratic coefficient is ∼0.1% the level of the linear coefficient. Given that the linear shift is already small, it is likely that if the boundary shift truly is quadratic, that this is not observable in experimental data.

Although we have not described a model dealing with the serial direction, it is observed that under normal gate biasing conditions correlations in the parallel direction are much larger than those in the serial direction. Assuming that the boundary shift is in fact linear with charge, then we can estimate the nonlinearity of the photon transfer curve β using the equation from Guyonnet:

$$\beta = -\sum_x a^x_{00} \tag{21}$$

Though we only have access to two of the necessary 4 terms, we should find that our estimates of β are low but comparable to experimental data. We are particularly interested in whether the value of this quantity changes with back side bias as our model predicts (Figure 8)

5. EXPERIMENTAL MEASUREMENTS

Although the ideal experimental test of correlated charge collection effects is probing the impulse response of the CCD directly by projecting small light spots onto pixels, it is experimentally much simpler to measure the statistics of flat field illumination, including the nonlinearity of the Photon Transfer Curve (PTC) and spatial

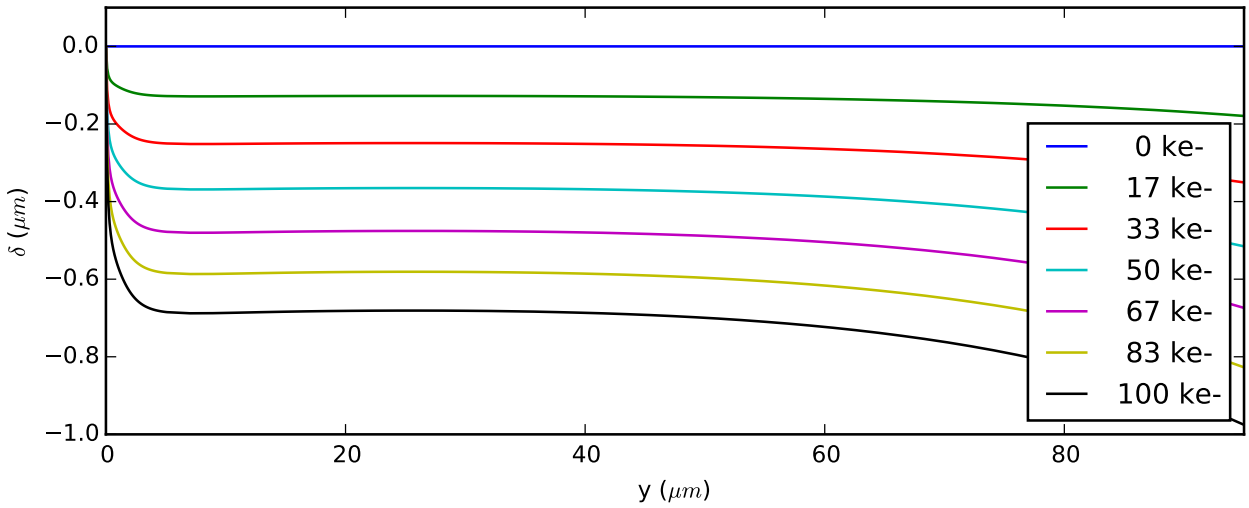

Figure 7. Pixel boundary shift calculations for $V_G = 80\,\mathrm{V}$, $V_T = 70\,\mathrm{V}$, with varying amounts of charge stored in the central pixel

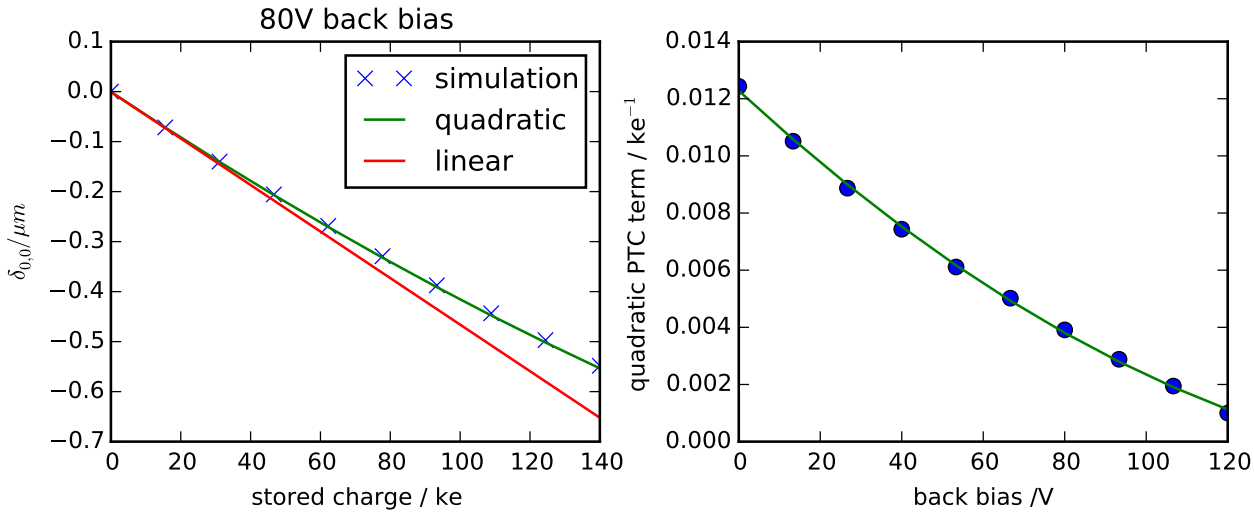

Figure 8. calculations of average boundary shift for different stored charges (left), and the expected nonlinearity terms of the PTC for varying back side bias (right)

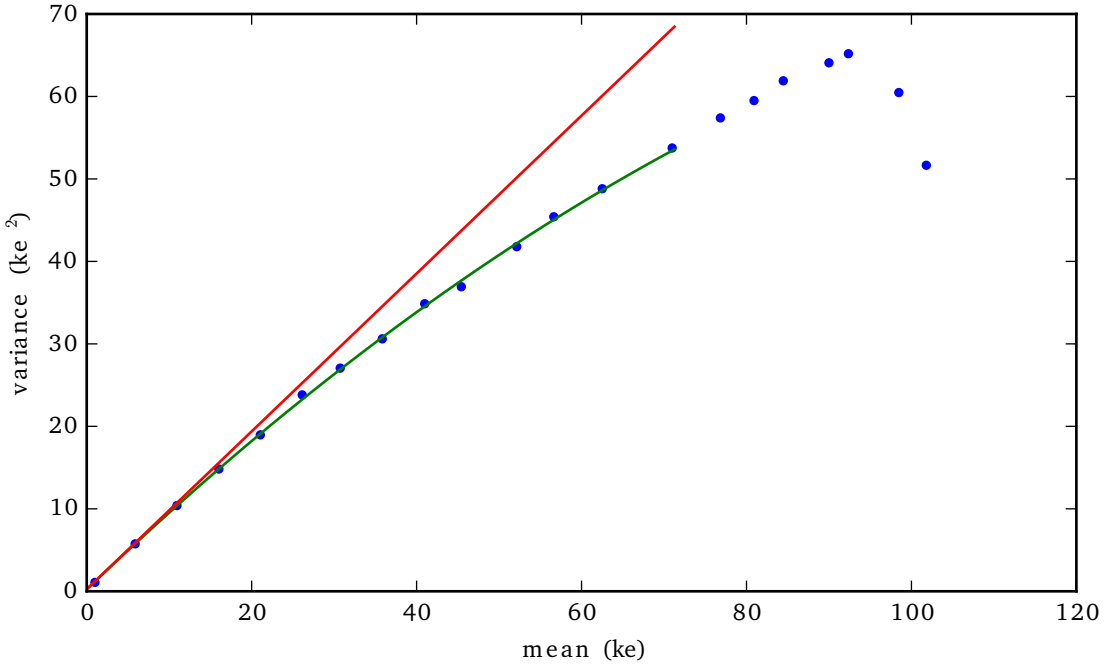

Figure 9. Example PTC from the CCD250, taken at backside bias of -10V, and wavelength of 827 nm. The green line shows the quadratic fit used for calibration, and the red line the mean=variance line.

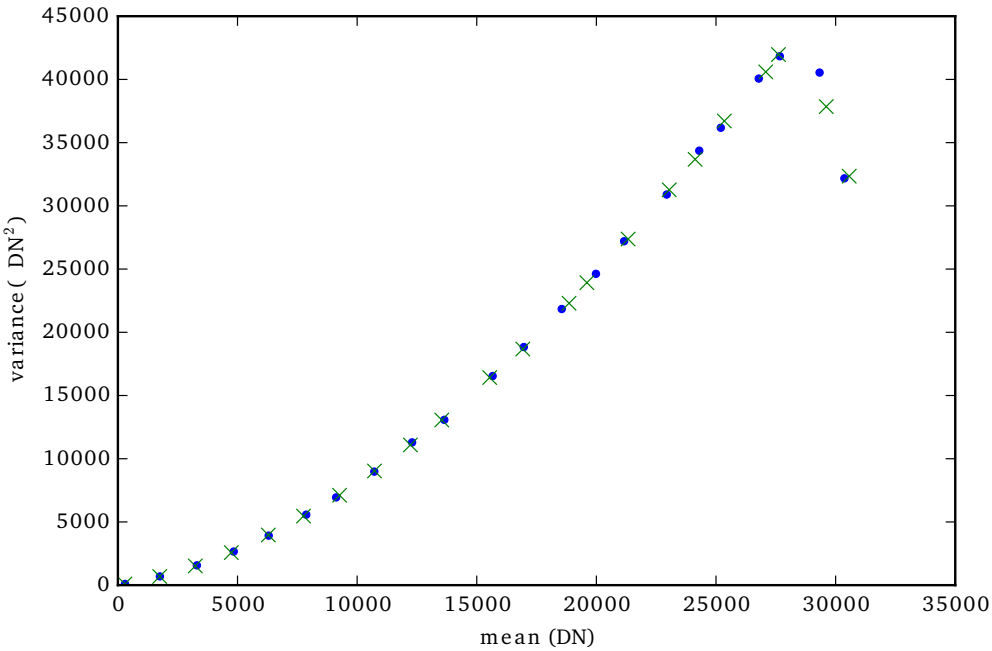

Figure 10. Raw PTC curve before frame differencing. The dots show the first exposure in a pair, the crosses the second exposure. Note that though all points lie on the same curve, there are noticeable discrepancies between the mean values of some first and second frames. Significant contribution from Fixed Pattern Noise (FPN) is not cancelled by the subtraction of such frame pairs.

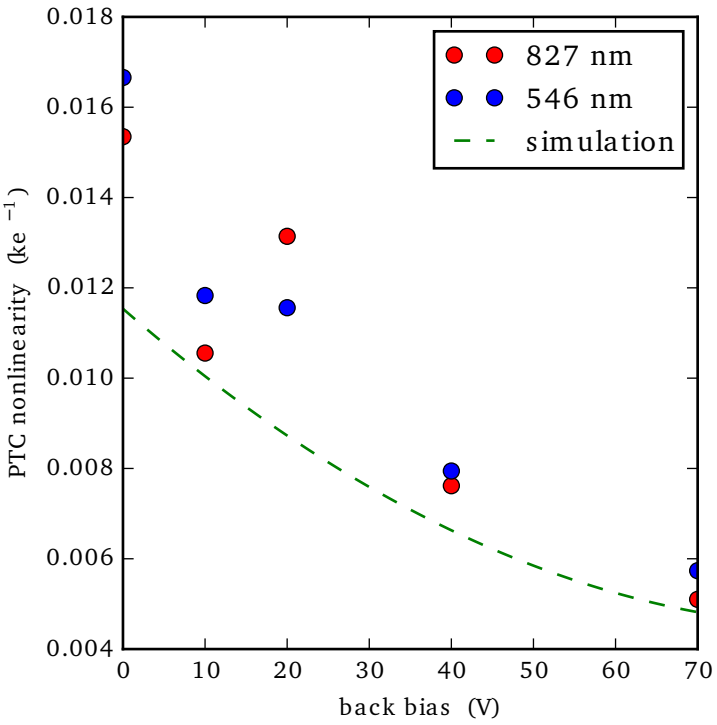

Figure 11. Measured PTC nonlinearities at different back substrate voltages. As expected, the simulation values consistently underestimate the nonlinearity due to not including the serial direction components

autocorrelation. It seems that necessary ancillary pixel data for BFE compensation is also available by this method.[5]

PTCs were taken on an e2v CCD250 cooled to $-100\,^{\circ}$C at Brookhaven National Laboratory. Measurements were collected for 5 different backside bias voltages from 0V to -70V, and at two wavelengths, selected using a monochromator. An example PTC is shown in Figure 9. Image pairs were taken at 32 exposure times for each PTC. Around 10 bias frames were also taken for each curve, and subtracted from each frame before differencing. The curves were fit using the expression

$$\sigma_s^2 = \beta \langle s \rangle^2 + \frac{\langle s \rangle}{K} \tag{22}$$

with $\langle s \rangle$ the average signal, σ_s^2 the spatial variance, K the camera gain, and β the PTC nonlinearity. The full well capacities observed in our data are much lower than that reported for other CCD250 devices tested in the literature (around 140ke-), though it is not known whether this is due to the operating conditions or a manufacturing defect in the particular device tested.

Unfortunately, slight fluctuations in the illumination level between exposures appear to be present in the dataset (see Figure 10). Frame pairs where a >1% discrepancy in mean value between the frames were not used in calibration or PTC fitting, but the resulting differenced frames did not provide enough statistics to accurately measure pixel to pixel correlation values. The measured values for the nonlinearity parameter β, however, do still appear to show reasonable agreement with our model (see Figure 11).

6. CONCLUSIONS

We have presented a method of solving the Poisson equation in a fully depleted, thick CCD which shows at least qualitative agreement with experiment in predicting some aspects of the brighter-fatter effect. There is, however, still much further work to complete. A much more sensitive experimental evaluation is required, and covering a larger parameter space (including the influence of front substrate voltage, and the phases used to collect charge, the effects of both of which are in principle calculable by the model). Verification against finite element simulations including solution of the continuity equations as well as the Poisson equation are also necessary to validate the accuracy of the model.

Work is ongoing to adapt the Green's function solution to include the effects in the serial direction of the device, which will lead to a more useful and full model. We are also performing random walk calculations based on the solutions presented here, which can be used to predict device PSF. The high fields in the device are likely to necessitate inclusion of velocity saturation, which is also at present not included.

It is nevertheless hoped that the work presented may be of use in evaluating device parameters for future applications where correlated charge collection effects are relevant.

REFERENCES

[1] M. Szafraniec, S.-M. Niemi, D. Walton, and M. Cropper, "On-ground characterization of the euclid low noise ccd273 sensor for precise galaxy shape measurements," *Journal of Instrumentation* **10**(01), p. C01030, 2015.

[2] I. Swindells, R. Wheeler, S. Darby, S. Bowring, D. Burt, R. Bell, L. Duvet, D. Walton, and R. Cole, "Mtf and psf measurements of the ccd273-84 detector for the euclid visible channel," 2014.

[3] E. A. H. Allanwood, N. J. Murray, K. D. Stefanov, D. J. Burt, and A. D. Holland, "Point-spread function and photon transfer of a ccd for space-based astronomy," *Proc. SPIE* **8860**, pp. 88600I–88600I–9, 2013.

[4] P. Antilogus, P. Astier, P. Doherty, A. Guyonnet, and N. Regnault, "The brighter-fatter effect and pixel correlations in ccd sensors," *Journal of Instrumentation* **9**(03), p. C03048, 2014.

[5] A. Guyonnet, P. Astier, P. Antilogus, N. Regnault, and P. Doherty, "Evidence for self-interaction of charge distribution in charge-coupled devices," *Astronomy & Astrophysics* **575**, p. A41, 2015.

[6] A. Rasmussen, P. Antilogus, P. Astier, C. Claver, P. Doherty, G. Dubois-Felsmann, K. Gilmore, S. Kahn, I. Kotov, R. Lupton, P. O'Connor, A. Nomerotski, S. Ritz, and C. Stubbs, "A framework for modeling the detailed optical response of thick, multiple segment, large format sensors for precision astronomy applications," 2014.

[7] Y. Yin and J. Cooper, J.A, "Simple equations for the electrostatic potential in buried-channel mos devices," *Electron Devices, IEEE Transactions on* **39**, pp. 1770–1772, Jul 1992.

[8] D. Weatherill, K. Stefanov, A. Holland, and D.Jordan, "Analytical investigation of correlated charge collection in ccds," *Journal of Instrumentation* **10**(02), p. C02002, 2015.

[9] S. M. Sze and K. K. Ng, *Physics of semiconductor devices*, Wiley-interscience, 2006.

[10] T. P. Lester and D. Pulfrey, "A new method based on the superposition principle for the calculation of the two-dimensional potential in a buried-channel charge-coupled device," *Electron Devices, IEEE Transactions on* **31**, pp. 999–1001, Jul 1984.

[11] J. Kevorkian, *Partial differential equations: Analytical solution techniques*, vol. 6, Springer Science & Business Media, 2000.

[12] D. Levin, "Development of non-linear transformations for improving convergence of sequences," *International Journal of Computer Mathematics* **3**(1-4), pp. 371–388, 1972.

[13] B. Gough, *GNU scientific library reference manual*, Network Theory Ltd., 2009.

[14] M. Downing, D. Baade, P. Sinclaire, S. Deiries, and F. Christen, "Ccd riddle: a) signal vs time: linear; b) signal vs variance: non-linear," 2006.